Friction **8**(1): 198–207 (2020)
https://doi.org/10.1007/s40544-019-0278-2
ISSN 2223-7690
CN 10-1237/TH
RESEARCH ARTICLE

Analysis of the high-temperature dry sliding behavior of $CoCrFeNiTi_{0.5}Al_x$ high-entropy alloys

Azmi ERDOĞAN[1,*], Mustafa Sabri GÖK[2], Sakin ZEYTIN[3]

[1] *Department of Metallurgy and Materials Engineering, Faculty of Engineering, Bartın University, Bartın 74100, Turkey*

[2] *Department of Mechanical Engineering, Faculty of Engineering, Bartın University, Bartın 74100, Turkey*

[3] *Department of Metallurgy and Materials Engineering, Faculty of Engineering, Sakarya University, Sakarya 54100, Turkey*

Received: 11 October 2018 / Revised: 3 December 2018 / Accepted: 13 January 2019

Abstract: In this study, $CoCrFeNiTi_{0.5}Al_x$ high-entropy alloys were produced by induction melting and their dry sliding wear behavior was examined at different temperatures. In addition to face-centered cubic (FCC) phases, low amounts of a tetragonal phase were detected in the microstructures of alloys without Al and microscratches were formed by wear particles on the worn surfaces of the alloy specimens. Two body-centered cubic (BCC) phases were detected in the alloy with 0.5Al and a fatigue-related extrusion wear mechanism was detected on the worn surface. The alloy specimen with a high Al content exhibited the best wear characteristics. No wear tracks were formed in single-phase BCC intermetallic alloys at room temperature and they exhibited a higher wear strength at high temperatures when compared to other samples.

Keywords: high-entropy alloy; dry sliding wear; friction; intermetallic

1 Introduction

Recently, new alloy systems, named high-entropy alloys (HEAs), with multiple principal elements were developed by Yeh et al. [1]. HEAs are advanced materials and their uniqueness lies in the fact that there is no single dominating element; all principal elements (> 5) have equal or near-equal atomic ratios in disordered solid solutions. The term "high-entropy" is based on the hypothesis that the enthalpy of formation can be overcome via a high enthalpy of mixing, thus enabling the formation of simple solid solutions [2–6]. In solid solutions, the entropy of mixing increases upon increasing the number of alloy elements. When five or more alloy elements are involved, the contribution of the entropy of mixing to the total free energy becomes significant, which in turn stabilizes the solutions. Accordingly, alloys with five or more elements are referred to as high-entropy alloys, and provide the ratio of each element in the alloy in the range of 5%–35% [7, 8].

Numerous studies on these alloys reported that they exhibited unique microstructures and superior characteristics [9–11]. Wu et al. [12] investigated the effect of Al addition to high-entropy CoCrCuFeNi alloys on their adhesive wear behavior. They reported that increasing the Al ratio increased the proportion of the body-centered cubic (BCC) phase as well as the alloy hardness. Moreover, increasing the Al ratio reduced the coefficient of friction (COF) and resulted in a shift from delamination wear to oxidative wear. Unnikrishnan et al. [13] investigated the effect of Co, Ti, and Si addition on the wear characteristics of AlCuNiFe alloys. Among these alloys, the highest hardness was obtained upon the addition of Si and Ti. In addition, the wear resistance of these HEAs was superior to that of conventional alloys. Wang et al. [14] investigated the effect of nitriding on the wear resistance of high-entropy AlCoCrFeNi alloys. Reportedly, the alloy hardness improved from 522 HV

* Corresponding author: Azmi ERDOĞAN, E-mail: erdogan@personel.bartin.edu.tr

to 720 HV upon nitriding. The researchers also stated that the nitride layer exhibited a significantly better wear resistance as compared to the cast alloy in dry sliding conditions. Yadav et al. [15] investigated the effect of Pb addition to AlCrFeMnV and Bi addition to CuCrFeTiZn with respect to the alloy dry sliding wear performance. It was observed that Pb addition did not induce any changes in the COF, whereas Bi addition resulted in a decrease in the COF. Increasing the Pb and Bi ratios resulted in a decrease in the wear rate by 21% and 25%, respectively. Yu et al. [16] investigated the wear behavior of $AlCoCrFeNiTi_{0.5}/Si_3N_4$ and $AlCoCrFeNiCu/Si_3N_4$ tribo-pair with compatible alloy and self-lubricating counterpart. They found that the tribo-chemical reactions of the HEA/Si_3N_4 couple could inhibit mechanical wear and improve tribological properties with increasing concentration of H_2O_2 solution. Numerous studies have been conducted on the wear characteristics of HEAs and almost all of them reported a high wear resistance [17–22]. On the other hand, only a limited number of reports are available on the high-temperature wear resistance of HEAs. These alloys are expected to exhibit superior high-temperature performance owing to a sluggish diffusion effect, which is one of the four "core effects" of HEAs [9, 23]. In this regard, the present study investigates the microstructural characteristics and high-temperature dry sliding wear behavior of high-entropy $CoCrFeNiTi_{0.5}Al_x$ alloys.

2 Experimental details

Alloy ingots with a nominal composition of $CoCrFeNiTi_{0.5}Al_x$ (x = 0, 0.5, and 1 corresponding to 0, 10, and 18.18 at%, respectively) were synthesized by induction melting using a mixture of pure metals powders (35 μm–44 μm size and of purity > 99.8%). The densities of samples were 7.85 g/cm^3, 7.37 g/cm^3, and 6.94 g/cm^3, respectively. The Co, Cr, Fe, Ni, Ti, and Al powders were initially mixed into the desired composition. The mixing was carried out at room temperature for 3 hours at a rotational speed of 200 rpm. After mixing, the powder mixture was cold pressed to form a cylindrical compact in a metallic mold under a uniaxial pressure of 200 MPa prior to casting. The chemical compositions of the produced alloys are included in Table 1. The molten alloys were cast into thin stainless steel molds with copper bottoms and cross-sectional dimensions of 60 mm × 30 mm. The entire induction casting system, including the crucible and molds, was kept in a controlled argon atmosphere during the melting and casting process for the preparation of $CoCrFeNiTi_{0.5}Al_x$ alloy ingots.

A scanning electron microscope (SEM, TESCAN MAIA3 XMU) was used to analyze the worn and metallographic alloy surfaces. A 3D optical profilometer (HUVITZ HDS-5800) was used for wear-depth and wear-loss measurements. Crystal structures in the samples were identified by X-ray diffraction (XRD, RIGAKU D/MAX/2200/PC) with Cu Kα radiation at an operating voltage and current of 40 kV and 30 mA, respectively. The scanning angle (2θ) was in the range of 20°–90°. Alloy microhardness measurements were conducted on a QNESS Q10 instrument (Austria) with a load of 100 g and dwell time of 15 s. The averages of measurements from 5 different points are shown on the Vickers scale.

Table 1 Chemical compositions of the as-solidified $CoCrFeNiTi_{0.5}Al_x$ alloys in atomic percentage (%).

Alloy	Region	Co	Cr	Fe	Ni	Ti	Al
$CoCrFeNiTi_{0.5}$	Dark(1)	21.7	24.2	24.2	22.2	8.9	—
	Gray(2)	22.4	25.3	22.3	17.6	12.4	—
	Light(3)	21.9	26.6	23.2	16.1	12.2	—
	Nominal	22.2	22.2	22.2	22.2	11.11	—
$CoCrFeNiTi_{0.5}Al_{0.5}$	Dark(1)	21.8	13.8	17.1	24.4	10.7	12.2
	Light(2)	15.1	36.4	30.3	9.3	4.6	4.3
	Nominal	20	20	20	20	10	10
$CoCrFeNiTi_{0.5}Al$	Matrix(1)	15.7	23.5	20.3	16.4	8.9	15.2
	Grain B.(2)	14.6	28.1	21.4	13.2	8.3	14.4
	Nominal	18.18	18.18	18.18	18.18	9.09	18.18

The dry sliding wear behavior of the samples was tested with WC abrasive balls of 6 mm diameter on a ball-on-disc tribometer. Wear tests were conducted at 25 °C, 250 °C, and 500 °C with a 10 N load over a total distance of 216 m. To ensure the accuracy of the results, each test was repeated three times and the mean values were obtained. After the wear tests, cross-sectional images of the wear marks were captured with an optical profilometer (Fig. 1) at four different points. To calculate the loss-of-volume wear in each sample, the average of 4 area measurements was multiplied by the diameter of the circular wear track.

3 Results and discussion

3.1 Microstructure of the as-solidified $CoCrFeNiTi_{0.5}Al_x$ alloys

The XRD patterns of the as-solidified alloys are shown in Fig. 2 and the identified phases with their lattice parameters are listed in Table 2. Two FCC phases and a tetragonal phase with weak peaks were found in the $CoCrFeNiTi_{0.5}$ sample. The lattice constants calculated from the XRD data were 3.603 Å and 3.590 Å for the A1 disordered (FCC1) phase and $L1_2$ ordered (FCC2) phase, respectively. Whereas the lattice constants of $D8_b$ (tetragonal) phase were *a*: 8.795 Å and *c*: 4.555 Å. The addition of Al, which has a large atomic radius (10 wt.%) and high affinity into the alloy sample induced changes in all the phases observed in the $CoCrFeNiTi_{0.5}$ alloy. A2 disordered (BCC1) and B2 ordered (BCC2) phases were detected in the $CoCrFeNiTi_{0.5}Al_{0.5}$ alloy. With the addition of Al, a new phase containing the Al-Ni-Ti atoms has occurred and replaced the FCC phases. The addition of Al, due to its high negative mixing enthalpy values with Ni and Ti elements caused a new phase formation, namely B2 (BCC2) in the alloy. The lattice constants of these phases were calculated from their Bragg peaks as 2.879 Å and 2.923 Å, respectively. With an increase in the Al ratio in high-entropy $CoCrFeNiTi_{0.5}Al$ alloys. The peaks belonging to the A2 phase disappeared, whereas highly intense peaks corresponding to the B2 disordered (BCC2) phase remained. The lattice constant of this phase was 2.901 Å.

Figure 3 presents the back-scattered electron SEM micrographs of the considered $CoCrFeNiTi_{0.5}Al_x$ HEAs. Table 2 outlines the chemical compositions of the cast alloys (analyzed by energy dispersive X-ray analysis (EDS)). Dendrite and inter-dendrite structures were observed in the $CoCrFeNiTi_{0.5}$ alloy. A phase with whisker-like distribution was observed in the light gray phase at high magnifications. From the XRD results, it can be inferred that this phase, which exhibits a low relative intensity, is most likely the tetragonal sigma phase. The light phase includes around 9% Ti with other elements being present in similar ratios. In the gray phase, the ratio of Ti was slightly higher than that of Ni. No significant changes were observed in the ratios of other elements. Typical dendritic and inter-dendiritic structures were observed in the $CoCrFeNiTi_{0.5}Al_{0.5}$ specimen. As shown in Fig. 2, the $CoCrFeNiTi_{0.5}Al_{0.5}$ alloy is composed of two BCC phases. The higher relative intensity of the BCC2 phase when compared to BCC1 is indicative of the lower weight ratio of the former. Thus, BCC1 corresponds

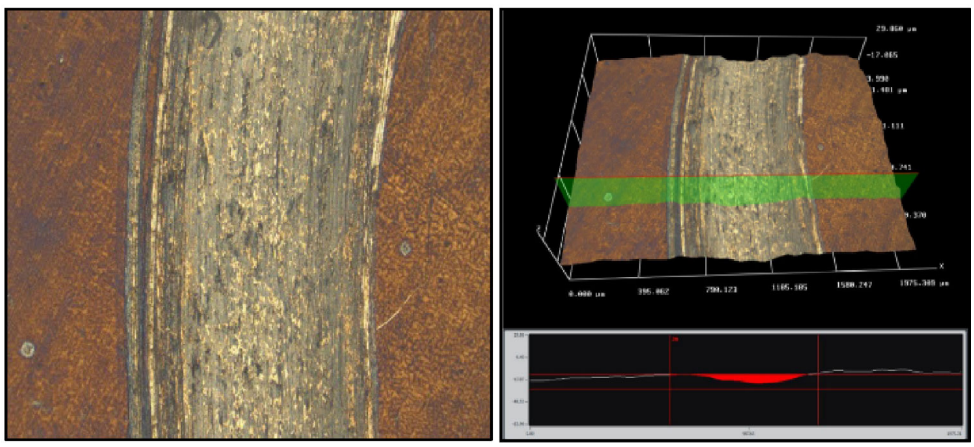

Fig. 1 Cross-sectional images of the wear marks observed using a 3D profile meter.

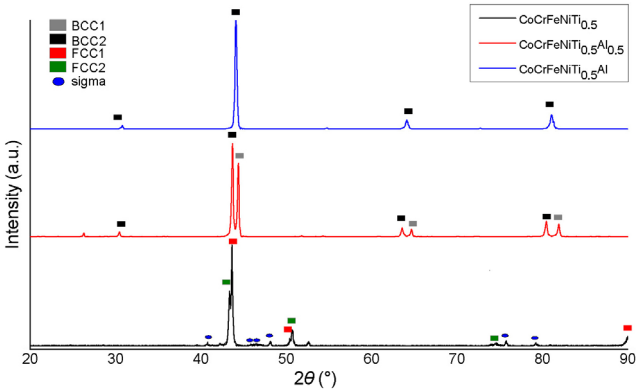

Fig. 2 XRD patterns of the as-solidified $CoCrFeNiTi_{0.5}Al_x$ alloys.

Table 2 Phases and lattice constants of the as-solidified $CoCrFeNiTi_{0.5}Al_x$ alloys as detected by XRD analysis.

Alloy	Lattice (Crystal structure)	Lattice parameter (Å)
$CoCrFeNiTi_{0.5}$	FCC1(A1) Fe-Ni	3.603 ± 0.006
	FCC2($L1_2$) Co-Ti	3.590 ± 0.005
	Tetragonal($D8_b$) Sigma	a = 8.795 ± 0.022. c = 4.555 ± 0.012
$CoCrFeNiTi_{0.5}Al_{0.5}$	BCC1(A2) Fe-Cr	2.879 ± 0.002
	BCC2(B2) Al-Ni-Ti	2.923 ± 0.002
$CoCrFeNiTi_{0.5}Al$	BCC2(B2) Al-Ni-Ti	2.901 ± 0.001

to the light phase, while BCC2 represents the dark phase as shown in Figs. 3(c) and 3(d). As indicated by the EDS results in Table 1, the dark phase is rich in Al-Ni-Ti, whereas the light phase has a high Fe and Cr content. Al, Ni, and Ti aggregate due to a large negative enthalpy of mixing, whereas the Fe-Cr rich phase precipitates in the vicinity of the dark phase due to its high concentration. A single-phase microstructure is observed in the $CoCrFeNiTi_{0.5}Al$ alloy specimen; this observation is supported by the XRD results. The amount of BCC2 phase increased due to the increase in the Al ratio. Probably due to this increase, Fe and Cr atoms were dissolved in this phase instead of forming a new phase, and as a result, a single phase microstructure was obtained. Equiaxed grains with an average size of 30 microns–35 microns were formed in this alloy. An even elemental distribution was observed in the grains, whereas slight changes were observed at the grain boundaries. However, the EDS results reflect approximate measurements conducted in a cross-sectional area corresponding to a diameter of 1 micron.

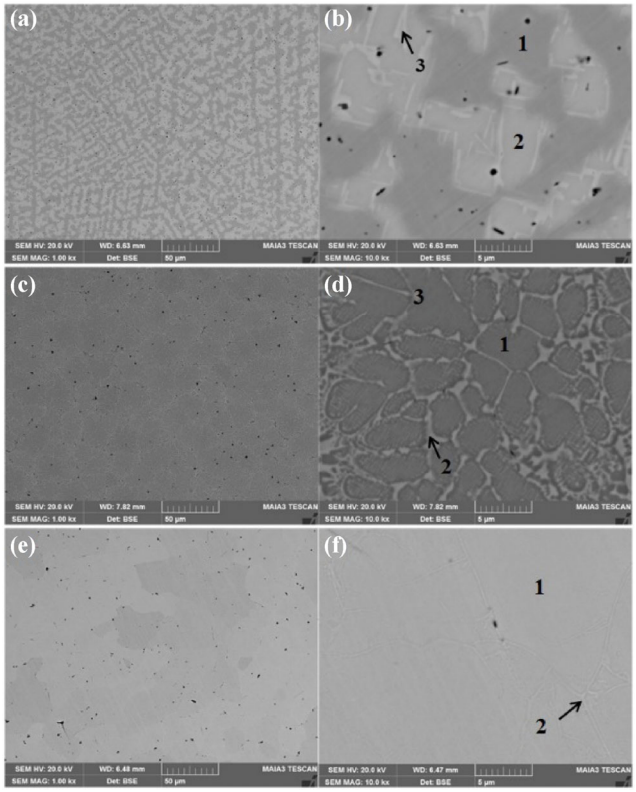

Fig. 3 SEM backscattered electron images of as-solidified $CoCrFeNiTi_{0.5}Al_x$ alloys. (a, b) Low- and high-magnification images of $CoCrFeNiTi_{0.5}$, respectively. (c, d) Low- and high-magnification images of $CoCrFeNiTi_{0.5}Al_{0.5}$, respectively. (e, f) Low- and high-magnification images of $CoCrFeNiTi_{0.5}Al$, respectively.

3.2 Hardness and dry sliding wear analysis

The volume loss graphs of the tested specimens are shown in Fig. 4. As shown in the figure, the highest wear resistance was observed on the $CoCrFeNiTi_{0.5}Al$ specimen. followed by the $CoCrFeNiTi_{0.5}Al_{0.5}$ and $CoCrFeNiTi_{0.5}$ specimens. $CoCrFeNiTi_{0.5}Al$ exhibited the best wear performance at high temperatures. Moreover, the wear volumes of this specimen at

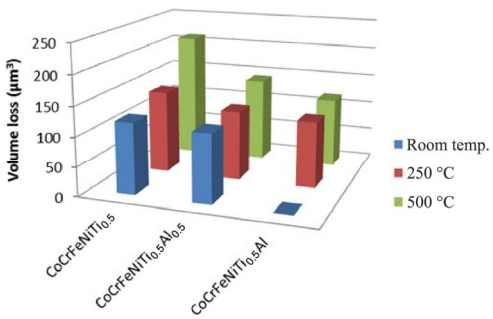

Fig. 4 Volume loss values of test samples at different sliding temperatures.

250 ˚C and 500 ˚C were close to the room-temperature values of other specimens.

Figure 5 shows the variations occurring in alloy hardness with respect to aluminum content. As the aluminum content increased, the hardness value increased. Observing the microstructural changes shown in Figs. 3 and 4. It can be concluded that alloy hardness is influenced by the phase type. Crystal structure transformation in the alloys from FCC to BCC caused a significant increase in the alloy hardness with an increase in the aluminum content. This indicates that the BCC phase is stronger than the FCC phase. This observation can be explained in two ways. The first is that slip along the closest packing planes {110} in the BCC structure is more difficult than that along the {111} planes in the FCC structure. {110} planes are less dense and more irregular. Therefore, a high lattice friction occurs during dislocation movement at the atomic scale. The second reason is that elements with strong binding forces, such as Al and elements with high melting temperatures, such as Cr, increase the Young's modulus and slip resistance [12]. Hence, it is apparent that aluminum not only exhibited strong binding forces with other metallic atoms but also a much larger atomic radius (1.4317 Å) [24]. Accordingly, increasing the Al ratio induced lattice distortion, which in turn increased the slip resistance. Moreover, the intermetallic $AlNi_2Ti$ phase, which was formed as a result of an increase in the Al ratio contributed to an increase in hardness. The wear volumes of the tested specimens clearly indicated that the highest hardness was exhibited by the $CoCrFeNiTi_{0.5}Al$ specimen. This statement is based on the definition of hardness—"it is the resistance against plastic deformation." $CoCrFeNiTi_{0.5}Al$ specimens, which exhibited the highest hardness, exhibited a high resistance to the action of the abrasive ball, resulting in a high wear resistance.

The friction coefficient graph obtained after conducting dry sliding wear tests on $CoCrFeNiTi_{0.5}$ alloys at three different temperatures with a 10 N load is shown in Fig. 6. The lowest COF was observed at room temperature and it increased with an increase in temperature. The specimens exhibited a stable COF at room temperature. At 250 ˚C, a low COF was observed for the first 600 s after which it increased. The COF at 500 ˚C was close to the value obtained at 250 ˚C. However, the value of the COF started to decrease after the first 1,200 s. From the SEM micrographs of the wear surfaces and COF graphs, it can be inferred that the COF observed in the initial wear stages is mainly due to an increase in the real contact area during the initial stages of the wear process. The more stabilized COF obtained after the removal of asperities can be ascribed to the formation of an oxide layer with superior mechanical characteristics when compared to the matrix material, which resulted in low wear rates. The oxide layer acted as a solid lubricant; in addition, work hardening also took place. The fluctuations observed in the COF during testing can be attributed to the fracture of the oxide layer formed on the surface and the wear debris that aggregated and adhered to the surface, thereby inducing additional resistance against the sliding of the abrading ball. This can be clearly observed in the SEM images in Fig. 7 in terms of the scratches on the

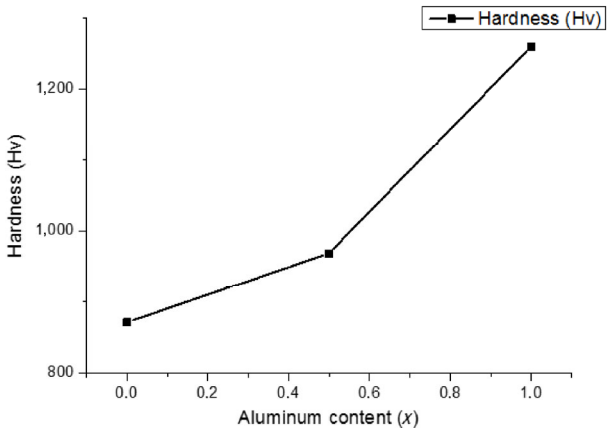

Fig. 5 Vickers hardness of $CoCrFeNiTi_{0.5}Al_x$ alloys with different aluminum content.

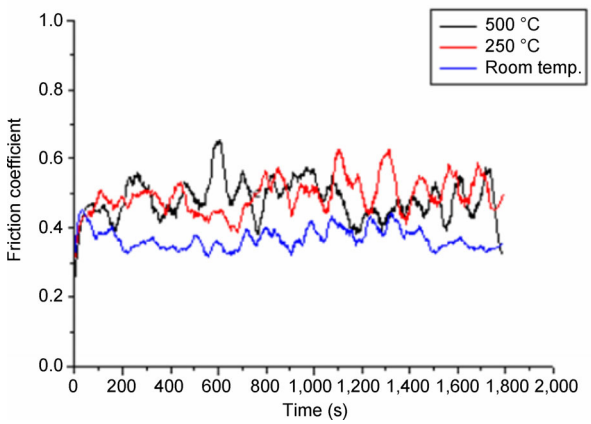

Fig. 6 Coefficient of friction of the $CoCrFeNiTi_{0.5}$ alloy as a function of sliding time at different temperatures.

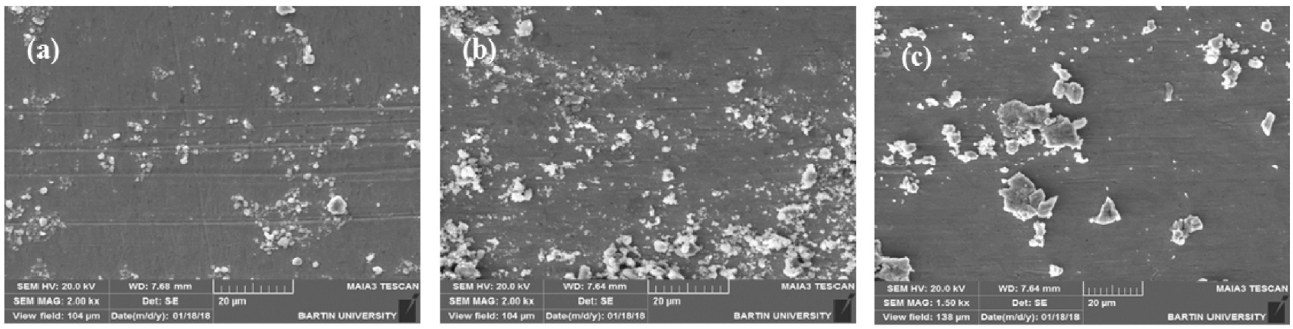

Fig. 7 SEM morphologies of the wear surfaces of $CoCrFeNiTi_{0.5}$ alloy specimens at (a) room temperature, (b) 250 ˚C, and (c) 500 ˚C.

surface due to detached particles.

The increased COF at 250 ˚C in addition to the difference in the peak amplitudes and heights obtained at this temperature when compared to the values at room temperature, are attributable to the increase in the rate of formation and spallation of the oxide layer at high temperatures. Figure 7 shows the morphologies of the wear surfaces of the $CoCrFeNiTi_{0.5}$ alloy after testing and the debris produced during the test. When compared to Fig. 7(a). More wear particles are observed in Fig. 7(b). Tests performed at the highest temperature resulted in relatively smooth worn surfaces with microscratches 20 μm–50 μm in size. Such low roughness can be ascribed to the reduced hardness of the specimens at high temperatures, thus resulting in a highly deformable surface. When the alloying elements of the sample are examined, Ti, Cr, and Fe are the elements with high probability for oxidation. With temperature increasing, these elements will more easily form oxidized compounds. Depending on the nature of this oxide layer forming on the surface, it will either be removed from the surface as wear debris or attached to the surface. The oxide particles detached from the surface can either form a load bearing barrier or cause the formation of micro-groove as it sinking into the surface like abrasive particles. When the image of the wear surface was carefully examined, it was seen that micro-grooves were formed at many points in short dimension.

As shown in the COF graph of the $CoCrFeNiTi_{0.5}Al_{0.5}$ alloy (Fig. 8). The COF values obtained at 250 ˚C were similar to those obtained at room temperature, but significantly higher values were obtained at 500 ˚C. The SEM micrograph (Fig. 9) of the worn surface after conducting the tests at 500 ˚C shows that the dominant wear mechanism is fatigue-induced extrusion. EDS

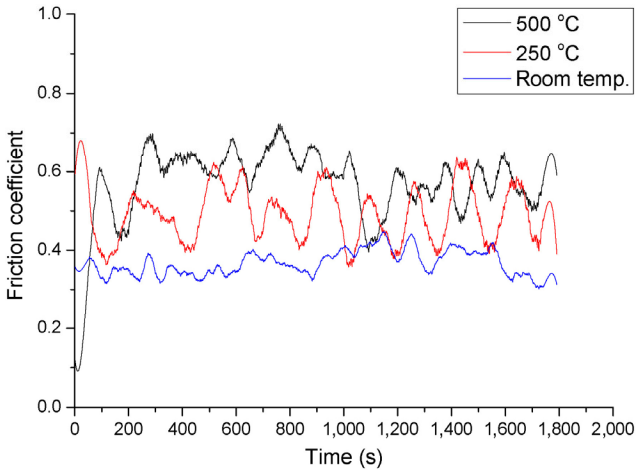

Fig. 8 Coefficient of friction of the $CoCrFeNiTi_{0.5}Al_{0.5}$ alloy as a function of sliding time at different temperatures.

analysis indicated a high oxygen content in the wear particles (Fig. 10). Roughening induced by extrusion on the surface resulted in significantly high COF values as compared to the others. Metallic tearings that occurred parallel to the wear track on the extruded surface were also effective in increasing the COF.

The $CoCrFeNiTi_{0.5}Al$ alloy on the other hand exhibited the lowest COF values among all the tested specimens (Fig. 11). Its COF value was initially stable at 250 ˚C, but began to increase after 700 s and stabilized at 500 ˚C. Fluctuation in the COF values at 250 ˚C is attributable to wear debris, whereas the fluctuation observed at 500 ˚C might have been induced by roughening caused by detached particles as a result of fatigue wear (Fig. 12) [19]. When the friction coefficients obtained at room temperature were examined, the lowest friction coefficient was observed. Only an increase during the first 100 s was observed. This is the condition seen during the cleaning of the surface roughness. Then the curve became more stable.

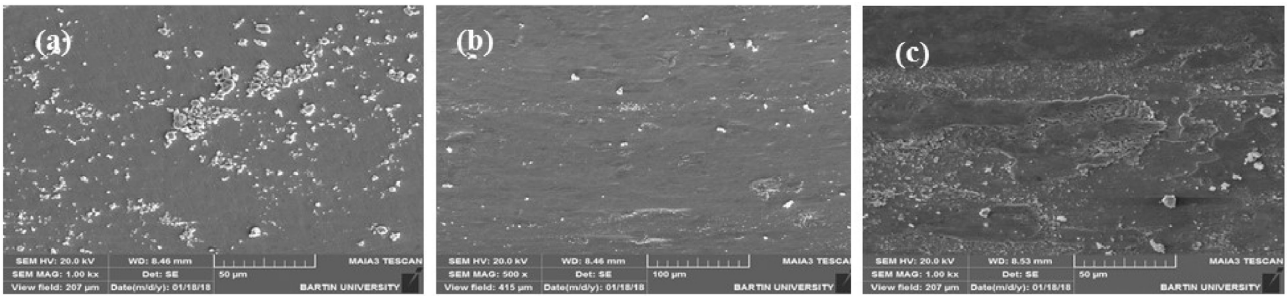

Fig. 9 SEM morphologies of the wear surface of the $CoCrFeNiTi_{0.5}Al_{0.5}$ alloy at (a) room temperature, (b) 250 ˚C, and (c) 500 ˚C.

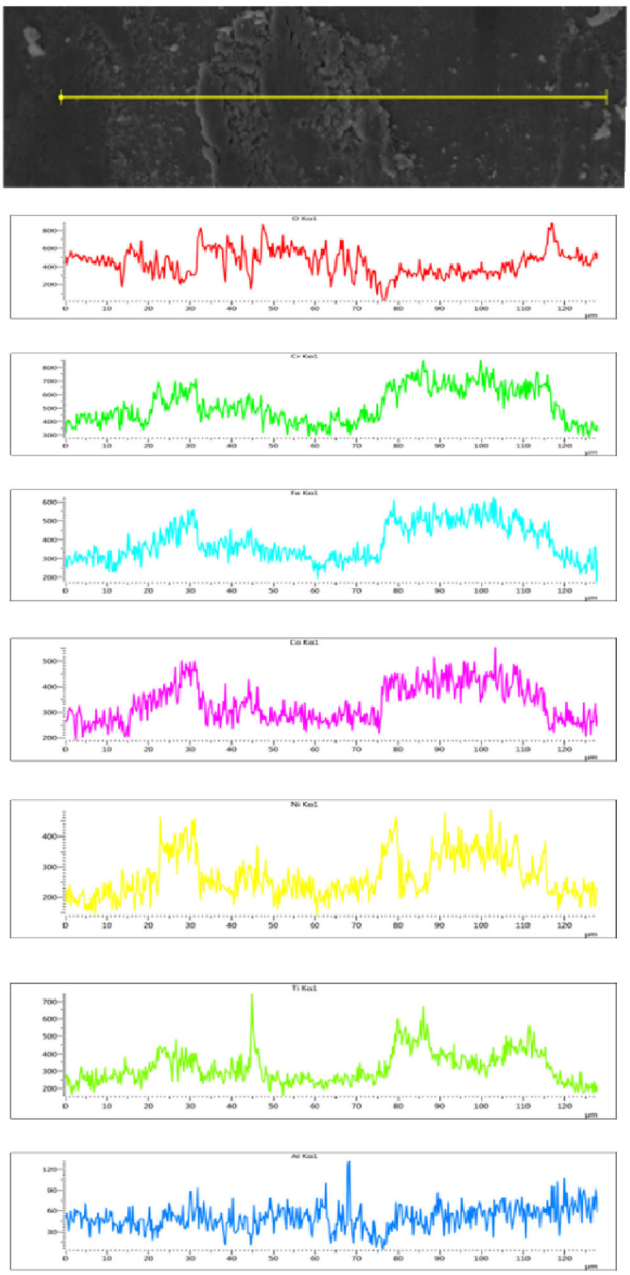

Fig. 10 EDS analysis of wear particles from the $CoCrFeNiTi_{0.5}Al_{0.5}$ alloy at 500 ˚C.

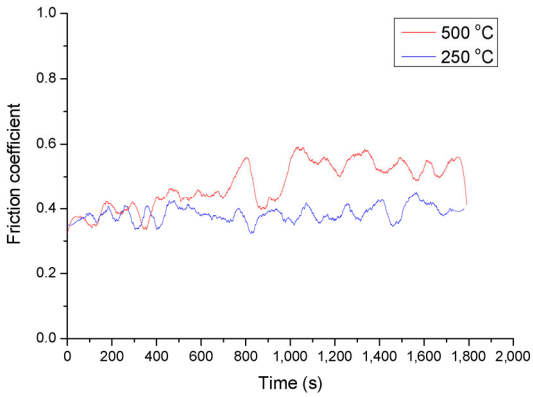

Fig. 11 Coefficient of friction of the $CoCrFeNiTi_{0.5}Al$ alloy as a function of sliding time at different temperatures.

At room temperature, the highest volume loss among all the specimens was observed for the $CoCrFeNiTi_{0.5}$ alloy, followed by $CoCrFeNiTi_{0.5}Al_{0.5}$ and $CoCrFeNiTi_{0.5}Al$ alloys. The XRD results and microstructures of the specimens indicate that the matrix of the $CoCrFeNiTi_{0.5}$ alloy is composed of soft and ductile phases, such as FCC1 + FCC2 [12, 21]. Additionally, the whisker-like intermetallic σ phase distributed within the matrix acted as a load bearing constituent, thereby contributing to a reduction in wear loss. Smooth surfaces with wear debris and micro-scratches formed due to this debris are observed in the SEM micrographs of this specimen's wear track. When compared to room-temperature values, no significant changes could be observed in the volume loss of the $CoCrFeNiTi_{0.5}$ alloy at 250 ˚C; however, it increased by approximately two times at 500 ˚C.

The $CoCrFeNiTi_{0.5}Al_{0.5}$ alloy exhibited superior wear resistance as compared to the $CoCrFeNiTi_{0.5}$ alloy. This is to be expected as the high resistance of the hard BCC1 + BCC2 phases towards plastic deformation and delamination might help the oxide layer withstand abrasion. The high wear resistance of the alloys at

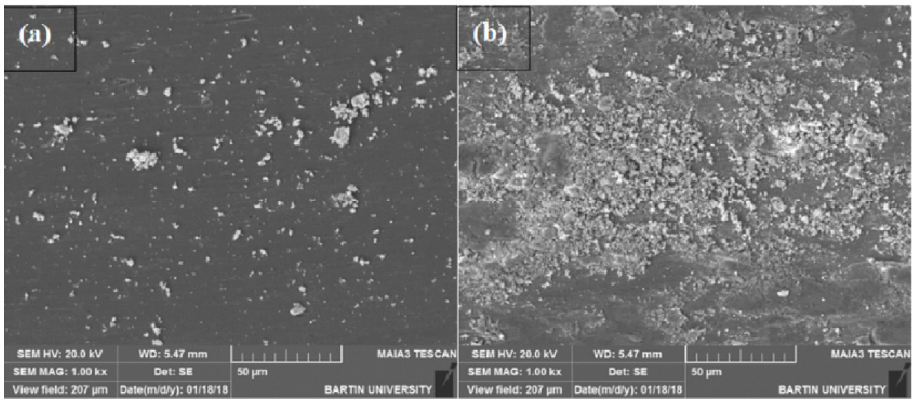

Fig. 12 SEM morphologies of the wear surface of the $CoCrFeNiTi_{0.5}Al$ alloy specimen at (a) 250 ˚C and (b) 500 ˚C.

high aluminum contents is ascribed to the oxide film, which is resistant to delamination [25]. Al_2O_3, which selectively formed during oxidation, slows down the rapid penetration of oxygen into the material. Alumina is a stable oxide that grows very slowly during oxidation and provides high resistance against oxygen penetration. It prevents exposure of the fresh surface as well as adhesive wear and thus prevents further wear damage [15, 26, 27]. It should be noted that the matrix grains of the $CoCrFeNiTi_{0.5}Al_{0.5}$ alloy consist of BCC2 (Al-Ni-Ti), whereas the intragranular phase surrounding these grains is the BCC1 (FeCr) phase. The BCC2 phase resists plastic deformation, whereas the BCC1 phase absorbs energy. During the metal metal interaction, the soft structural component is subjected to plastic deformation and the hard structural component is subjected to elastic deformation. With time passing, the hard phase occurs gradually. This causes a reduction in wear rate. However, the excessive amount of hard phase may cause the wear mechanism to return to fatigue [28]. Further, the stable structure of this intermetallic phase at high temperatures prevents high wear rates at elevated temperatures.

The $CoCrFeNiTi_{0.5}Al$ alloy exhibited the lowest volume loss among all the tested specimens. At room temperature, no significant wear loss was detected in this alloy. Moreover, the wear loss of this specimen at 500 ˚C was close to the wear loss of other alloy specimens at room temperature. The high wear resistance of this specimen is mainly ascribed to its microstructure, which consists of an intermetallic phase with significantly high strength and hardness [28].

4 Conclusions

In this study, high-entropy $CoCrFeNiTi_{0.5}Al_x$ alloys with varying aluminum content were produced by induction melting and analyzed by dry sliding wear tests at different temperatures. Upon increasing the aluminum content in $CoCrFeNiTi_{0.5}Al_x$ alloys, both the volume ratio of the strong BCC phase and the alloy hardness increased, which also led to an increase in the wear resistance and changed the wear mechanism. The $CoCrFeNiTi_{0.5}Al$ alloy exhibited the highest wear resistance among all the tested specimens. No wear tracks were formed at room temperature in these specimens; in addition, a high wear resistance was obtained due to the single-phase ordered BCC (Al-Ni-Ti) structure formed at high temperatures. A pull-out wear mechanism was observed as a result of high hardness and strength. Further, a high Al content resulted in stable oxides of Al, which contributed to alloy wear resistance. A moderate wear resistance was observed in both room-temperature and high-temperature tests for $CoCrFeNiTi_{0.5}Al_{0.5}$ alloy. In particular, the ordered BCC phase (Al-Ni-Ti) with its high hardness resulted in a superior wear resistance at both room temperature and high temperature during testing (these alloys contained two different BCC phases). A fatigue-induced extrusion wear mechanism was observed during alloy testing. Further, oxidative wear was detected during high-temperature alloy testing. Such behavior, which reflects a low wear resistance, is attributed to its composition with a high ductile FCC content; in addition, the micro-scratches observed on the worn surface of the alloy

can be ascribed to its ductile structure. The lack of Al, which forms stable oxides on the surface and acts as a BCC phase stabilizer, results in a low wear resistance at high temperatures.

References

[1] Yeh J W, Chen S K, Lin S J, Gan J Y, Chin T S, Shun T T, Tsau C H, Hang S Y. Nanostructured high-entropy alloys with multiple principal e lements: Novel alloy design concepts and outcomes. *Adv Eng Mater* **6**(5): 299–303 (2004)

[2] Laplanche G, Gadaud P, Horst O, Otto F, Eggeler G, George E P. Temperature dependencies of the elastic moduli and thermal expansion coefficient of an equiatomic, single-phase CoCrFeMnNi high-entropy alloy. *J Alloys Compb* **623**: 348–353 (2015)

[3] Liu W H, He J Y, Huang H L, Wang H, Lu Z P, Liu C T. Effects of Nb additions on the microstructure and mechanical property of CoCrFeNi high-entropy alloys. *Intermetallics* **60**: 1–8 (2015)

[4] Stepanov N D, Shaysultanov D G, Salishchev G A, Tikhonovsky M A, Oleynik E E, Tortika A S, Senkov O N. Effect of V content on microstructure and mechanical properties of the CoCrFeMnNiV_x high entropy alloys. *J Alloys Compd* **628**: 170–185 (2015)

[5] Wang Z Q, Wang X R, Yue H, Shi G T, Wang S H. Microstructure, thermodynamics and compressive properties of AlCoCrCuMn-*x* (*x*=Fe, Ti) high-entropy alloys. *Mater Sci Eng A* **627**: 391–398 (2015)

[6] Fu Z Q, Chen W P, Wen H M, Chen Z, Lavernia E J. Effects of Co and sintering method on microstructure and mechanical behavior of a high-entropy $Al_{0.6}$NiFeCrCo alloy prepared by powder metallurgy. *J Alloys Compd* **646**: 175–182 (2015)

[7] Gali A, George E P. Tensile properties of high- and medium-entropy alloys. *Intermetallics* **39**: 74–78 (2013)

[8] Erdogan A, Yener T, Zeytin S. Fast production of high entropy alloys (CoCrFeNiAl_xTi_y) by electric current activated sintering system. *Vacuum* **155**: 64–72 (2018)

[9] Zhang Y, Zuo T T, Tang Z, Gao M C, Dahmen K A, Liaw P K, Lu Z P. Microstructures and properties of high-entropy alloys. *Prog Mater Sci* **61**: 1–93 (2014)

[10] Tsai M H, Yeh J W. High-entropy alloys: A critical review. *Mater Res Lett* **2**(3): 107–123 (2014)

[11] Tian F Y, Varga L K, Chen N X, Shen J, Vitos L. Empirical design of single phase high-entropy alloys with high hardness. *Intermetallics* **58**: 1–6 (2015)

[12] Wu J M, Lin S J, Yeh J W, Chen S K, Huang Y S, Chen H C. Adhesive wear behavior of Al_xCoCrCuFeNi high-entropy alloys as a function of aluminum content. *Wear* **261**: 513–519 (2006)

[13] Unnikrishnan T G, Paul C, Sellamuthu R, Arul S. An investigation on the effects of Co, Ti and Si on microstructure, hardness and wear properties of AlCuNiFe based entropy alloys. *Mater Today Proc* **4**(2): 178–187 (2017)

[14] Wang Y X, Yang Y J, Yang H J, Zhang M, Ma S G, Qiao J W. Microstructure and wear properties of nitrided AlCoCrFeNi high-entropy alloy. *Mater Chem Phys* **210**: 233–239 (2018)

[15] Yadav S, Kumar A, Biswas K. Wear behavior of high entropy alloys containing soft dispersoids (Pb, Bi). *Mater Chem Phys* **210**: 222–232 (2018)

[16] Yu Y, Wang J, Yang J, Qiao Z H, Duan H T, Li J S, Li J, Liu W M. Corrosive and tribological behaviors of AlCoCrFeNi-M high entropy alloys under 90 wt.% H2O2 solution. *Tribol Int* **131**: 24–32 (2019)

[17] Cai Z B, Cui X F, Liu Z, Li Y, Dong M L, Jin G. Microstructure and wear resistance of laser cladded Ni-Cr-Co-Ti-V high-entropy alloy coating after laser remelting processing. *Opt Laser Technol* **99**: 276–281 (2018)

[18] Ayyagari A, Barthelemy C, Gwalani B, Banerjee R, Scharf T W, Mukherjee S. Reciprocating sliding wear behavior of high entropy alloys in dry and marine environments. *Mater Chem Phys* **210**: 162–169 (2018)

[19] Mathiou C, Poulia A, Georgatis E, Karantzalis A E. Microstructural features and dry-sliding wear response of MoTaNbZrTi high entropy alloy. *Mater Chem Phys* **210**: 126–135 (2018)

[20] Poletti M G, Fiore G, Gili F, Mangherini D, Battezzati L. Development of a new high entropy alloy for wear resistance: $FeCoCrNiW_{0.3}$ and $FeCoCrNiW_{0.3}$ + 5 at.% of C. *Mater Des* **115**: 247–254 (2017)

[21] Liu X T, Lei W B, Ma L J, Liu J L, Liu J, Cui J Z. Effect of boron on the microstructure, phase assemblage and wear properties of $Al_{0.5}CoCrCuFeNi$ high-entropy alloy. *Rare Metal Mater Eng*, **45**(9): 2201–2207 (2016)

[22] Sha M H, Zhang L, Zhang J W, Li N, Li T Z, Wang N. Effects of annealing on the microstructure and wear resistance of $AlCoCrFeNiTi_{0.5}$ high-entropy alloy coating prepared by laser cladding. *Rare Metal Mater Eng* **46**(5): 1237–1240 (2017)

[23] Stepanov N D, Shaysultanov D G, Salishchev G A, Tikhonovsky M A. Structure and mechanical properties of a light-weight AlNbTiV high entropy alloy. *Mater Lett* **142**: 153–155 (2015)

[24] Tong C J, Chen M R, Chen J W, Yeh J W, Lin S J, Chen S K, Shun T T, Chang S Y. Mechanical performance of the $Al_xCoCrCuFeNi$ high-entropy alloy system with multiprincipal elements. *Metall Mater Trans A* **36**(5): 1263–1271 (2005)

[25] Chuang M H, Tsai M H, Wang W R, Lin S J, Yeh J W. Microstructure and wear behavior of $Al_xCo_{1.5}CrFeNi_{1.5}Ti_y$ high-entropy alloys. *Acta Mater* **59**: 6308–6317(2011)

[26] Doleker K M, Ozgurluk Y, Karaoglanli A C. Isothermal oxidation and thermal cyclic behaviors of YSZ and double-layered YSZ/$La_2Zr_2O_7$ thermal barrier coatings (TBCs). *Surf CoatTech* **351**: 78–88 (2018)

[27] Kai W, Li C C, Cheng F P, Chu K P, Huang R T, Tsay L W, Kai J J. Air-oxidation of FeCoNiCr-based quinary high-entropy alloys at 700–900 °C. *Corros Sci* **121**: 116–125 (2017)

[28] Fox-Rabinovich G, Totten G E. *Self-Organization During Friction*: *Advanced Surface-Engineered Materials and Systems Design*. Florida (U.S.):CRC Press, 2006: 59–150.

[29] Yusenko K V, Riva S, Crichton W A, Spektor K, Bykova E, Pakhomova A, Tudball A, Kupenko I, Rohrbach A, Klemme A, et al. High-pressure high-temperature tailoring of High Entropy Alloys for extreme environments. *J Alloys Compd* **738**: 491–500 (2018)

Azmi ERDOĞAN. He was born in 1986 and graduated from Faculty of Chemical and Metallurgical Engineering, Yıldız Technical University in 2009. He received his Ph.D degree in material science and engineering in 2018 from Sakarya University. He began his career at Bartın University as a research assistant from 2010. His research interests include high-entropy alloys, ECAS, tribology, and surface technologies.

Mustafa SABRI GÖK. He is the head of Mechanical Engineering, Faculty of Engineering, Bartın University, Turkey. He graduated from Faculty of Technology, Fırat University in 1996. Prof. Gök received his Ph.D degree in 2008 from Fırat University. He became a professor in 2018. His research area is mainly about the friction and wear behavior of materials.

Sakin ZEYTIN. He was born in 1957 in Trabzon, Turkey. He received his bachelor degree in metallurgical engineering from Istanbul Technical University in 1980, master degree in 1982, and Ph.D in 1990, from ITU Institute of Science and Technology. He began his career at ITU as a research assistant (1982–1988). He worked in Çelikord Inc. as a quality engineer (1988–1989) and at TÜBİTAK as an expert researcher (1989–1993). In 1994, he joined Sakarya University. He became a professor in 2006. His research area is mainly about surface technology, intermetallics, and fracture analysis.